



# A hybrid analytical–numerical model for calculating the maximum elastic force acting on a flow-driven elastic prolate spheroidal particle during its collision with a rigid wall

Rongxuan Hu<sup>1</sup> · Yinshui Liu<sup>1</sup> · Jure Ravnik<sup>2</sup> · Matjaž Hriberšek<sup>2</sup> · Paul Steinmann<sup>3,4</sup> · Yan Cui<sup>1</sup>

Received: 22 August 2021 / Accepted: 24 November 2021

© The Author(s), under exclusive licence to Springer-Verlag GmbH Germany, part of Springer Nature 2021

## Abstract

The paper proposes a hybrid analytical–numerical model for calculating the maximum elastic force acting on a flow-driven prolate spheroidal particle during its collision with a rigid wall. This model assumes that the maximum elastic force is a function of normal impact velocity, particle material properties, particle size, particle aspect ratio and particle orientation angle. The relationship between the parameters is determined by dimensional analysis. The remaining unknown coefficients are calibrated by performing finite element (FE) simulations. The solutions for particle aspect ratios of 1.5, 2 and 3 are presented. The proposed model is verified by comparison with independent FE simulation results for different normal impact velocities, particle material properties, particle sizes, particle aspect ratios and particle orientation angles. The results of the comparison between the results of the proposed model and the FE simulation results show a good agreement for small deformations of the particle. The model is valid for any properties of particle material, particle sizes and particle orientation angles.

**Keywords** Prolate spheroidal particle · Elastic force · Finite element simulation · Non-spherical particle–wall collision · Hybrid analytical–numerical model

---

✉ Yan Cui  
yan\_cui@hust.edu.cn

Rongxuan Hu  
rongxuan\_hu@hust.edu.cn

Yinshui Liu  
liuwater@hust.edu.cn

Jure Ravnik  
jure.ravnik@um.si

Matjaž Hriberšek  
matjaz.hribersek@um.si

Paul Steinmann  
paul.steinmann@fau.de

<sup>1</sup> School of Mechanical Science and Engineering, Huazhong University of Science and Technology, Wuhan 430074, Hubei, China

<sup>2</sup> Faculty of Mechanical Engineering, University of Maribor, Smetanova 17, 2000 Maribor, Slovenia

<sup>3</sup> Institute of Applied Mechanics, Friedrich-Alexander Universität Erlangen-Nürnberg, Paul-Gordan-Str. 3, 91052 Erlangen, Germany

## 1 Introduction

In dispersed multiphase flow, the elastic force acting on a particle during its collision with a wall needs to be correctly determined in order to gain insight-seeing into the particle–wall interaction. For example, the deposition of particles on an adhesive surface arises from an energy balance by comparing the dissipation of kinetic energy of the particle with the incident kinetic energy, in which the elastic force plays an important role in the kinetic energy [15,23]; shot peening is used to produce a compressive residual stress layer and strengthen the surface of metals, and the elastic force acting on the particle is used to estimate the residual stress [13,24].

Most studies focus on the interaction between a spherical particle and a wall [1,8], whereas studies on non-spherical particle–wall collision are far less numerous, despite the fact that flows with non-spherical particles occur in many practical cases. One of the reasons for this lies in several difficulties in dealing with such multiphase systems:

<sup>4</sup> Glasgow Computational Engineering Centre, University of Glasgow, Glasgow, UK

- (1) It is difficult to derive an analytical model for calculating the elastic force acting on a non-spherical particle due to the increasing number of parameters. Unlike in the case of spherical particles, it is necessary to take into account the aspect ratio  $\lambda$  (i.e.  $\lambda = b/a$ , where  $b$  and  $a$  are the semi-major and the semi-minor axis of the particle, respectively) [7,21] as well as the orientation angle  $\beta$  of the non-spherical particle (i.e. measured from the angle between the major axis of the particle and the wall) [2].
- (2) The determination of the elastic force can be achieved by performing numerical simulations using particles with specific particle material properties, shapes, and sizes. Although this approach is straightforward, it always leads to a large number of numerical simulations. For example, in Cui et al. [4], the elastic force acting on a glass fibre was studied. The glass fibres had a uniform shape (i.e.  $\lambda = 22.4$ ) and size (i.e. particle volume equivalent diameter  $D_p = 3.29 \mu\text{m}$ ) and more than 200 FE simulations were performed in order to construct the elastic force model of the fibre. Therefore, it is currently not feasible to derive an elastic force model for arbitrary particle material properties and sizes by performing only direct numerical simulations.

Regarding the above observations, it is clear that combining the advantages of the generality of theoretical derivations with targeted results of direct numerical simulations could lead to the derivation of a general elastic force model by using FE simulations to determine the unknown model parameter values. Using this approach in the case of non-spherical particles, it would be possible to derive an elastic force model with a wide range of applicability.

The solution of the elastic force as a function of compression distance was initially given by Landau et al. [16] for small deformations of two elastic solid particles for arbitrary properties and sizes of particle material. Cui and Sommerfeld [6] took the force model of Landau et al. [16] as a basis and proposed an analytical solution for calculating the maximum elastic force acting on an elastic spherical particle during the collision with a rigid plane wall taking the particle impact velocity and impact angle into account. This model is verified by comparison with the FE simulation results in Fig. 4, and a good agreement is found for small deformations of the particle. The analytical solution to determine the changes in the translational and rotational velocities of the particle during the collision was also proposed by Cui and Sommerfeld [6]. In the non-spherical particle–wall collision, most studies calculate the elastic force acting on the particle by performing FE simulations. Fang et al. [9,10] calculated the elastic force acting on disk-like graphite particles by performing FE simulations at two fixed orientations, i.e. vertical and horizontal. The influence of the particle sizes and material properties on

the critical sticking velocity was studied. Cui et al. [4] calculated the maximum elastic force acting on a glass fibre at arbitrary particle orientation angles and found that the fibre tends to collide with the wall twice in a collision event if the orientation angle is larger than  $60^\circ$ .

Prolate spheroidal particles have been widely used to represent the shape of non-spherical particles, e.g. quartz sands [18,22], sludge flocs [5] and fibres [3,11]. In particular, a prolate spheroidal particle is identical to a spherical particle for aspect ratio  $\lambda = 1$ . Therefore, it would be advantageous to derive an analytical model as a template for the elastic force using the prolate spheroidal particle. The process of deriving the elastic force model for a prolate spheroidal particle is as follows: first, a general model is proposed using analogy arguments (Sect. 2); then the relationship between the various parameters is determined by dimensional analysis (Sect. 2); after that, the remaining unknown model parameter values are calibrated by performing FE simulations (Sect. 4). Finally, the proposed model is verified by comparison with independent FE simulation results (Sect. 4). In Sect. 5, the advantages and limitations of the proposed model are summarised.

## 2 Derivation of the elastic force model

As shown in Fig. 1, a prolate spheroidal particle with an impact velocity  $U_0$ , collides with a wall at an impact angle  $\alpha$  (i.e. measured from the angle between the direction of the impact velocity and the plane wall) and an orientation angle  $\beta$ . The normal impact velocity is  $U_N = U_0 \sin \alpha$ . During the collision, the elastic particle deforms, and its incident kinetic energy is transformed into elastic potential energy. This deformation induces an elastic force  $F_e$  acting on the particle away from the wall. The fluid dynamic drag force and gravity are much smaller than the elastic force (i.e. as shown in Fig. 5) and can therefore be neglected. The Hertz contact [14] is applied to simplify the collision process. Therefore, the particle is assumed to be an elastic body, and the plane wall is assumed to be rigid.

The analytical solution of the elastic force acting on an elastic spherical particle during its collision with a rigid plane wall was proposed by Cui and Sommerfeld [6]:

$$F_e(y) = \frac{4E_p \sqrt{R_p}}{3[1 - \sigma_p^2]} y^{\frac{3}{2}}, \quad (1)$$

where  $y$  is the compression distance, and  $\sigma_p$ ,  $E_p$ ,  $R_p$  are the Poisson's ratio, the Young's modulus and the radius of the particle, respectively. It is obvious that the maximum elastic force acting on the particle is reached at the maximum compression distance  $h = \max(y)$ , which is given by

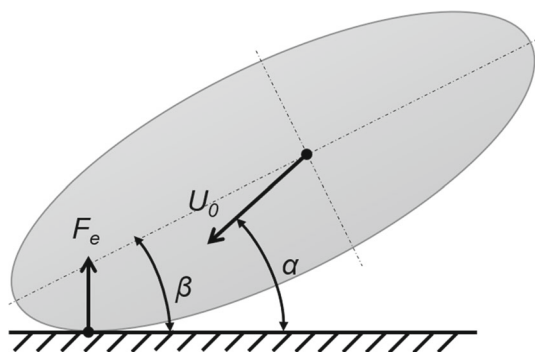


Fig. 1 A schematic diagram of the collision between a prolate spheroidal particle and a plane wall

$$h^{\frac{5}{2}} = \frac{15 m_p [U_0 \sin \alpha]^2}{16 \sqrt{R_p} \frac{1 - \sigma_p^2}{E_p}}, \quad (2)$$

where  $m_p$  is the mass of the particle. Therefore, the maximum elastic force acting on the spherical particle can be expressed as

$$F_{e,max} = 0.7574 \rho_p^{0.6} U_N^{1.2} D_p^2 \left[ \frac{E_p}{1 - \sigma_p^2} \right]^{0.4}. \quad (3)$$

The above equation demonstrates that the maximum elastic force acting on the particle is a function of the particle density  $\rho_p$ , the normal impact velocity, the volume equivalent diameter, Young’s modulus and the Poisson’s ratio. In the case of prolate spheroidal particles, the particle aspect ratio  $\lambda$  and orientation angle  $\beta$  are necessary to be taken into account. Therefore, a generalised form of the maximum elastic force model can be proposed as

$$F_{e,max} = \xi(\lambda, \beta) \rho_p^i U_N^j D_p^k \left[ \frac{E_p}{1 - \sigma_p^2} \right]^l \quad (4)$$

where  $i, j, k, l$  are exponents, and  $\xi(\lambda, \beta)$  is an unknown function of the particle aspect ratio and orientation angle. For any given particle aspect ratio and orientation angle,  $\xi(\lambda, \beta)$  has a dimensionless value.

In order to decrease the number of unknown parameters in Eq. (4), first a dimensional analysis is performed. The dimensions of mass, length and time are represented as {M}, {L} and {T}, respectively. Thus, Eq. (4) is written in terms of primary dimensions

$$\{MLT^{-2}\} = \{M^i L^{-3i}\} \{L^j T^{-j}\} \{L^k\} \{M^l L^{-l} T^{-2l}\}. \quad (5)$$

The dimensional analysis reveals that  $k = 2, j = 2i$  and  $l = 1 - i$ . Therefore, Eq. (4) can be simplified to

$$F_{e,max} = \xi(\lambda, \beta) \rho_p^i U_N^{2i} D_p^2 \left[ \frac{E_p}{1 - \sigma_p^2} \right]^{1-i} \quad (6)$$

In the case of spherical particles,  $\xi(\lambda = 1) = 0.7574$  and  $i = 0.6$ ; in the case of prolate spheroidal particles, the remaining unknown function  $\xi(\lambda, \beta)$  and exponent  $i$  can be determined by performing FE simulations.

### 3 Setup of finite element simulations

The non-linear FE simulations are performed by using the commercial software ABAQUS®. The Nlgeom (non-linear geometry) explicit dynamics solver is applied. Before the deformation, a Dirichlet boundary condition [20] is applied on the particle; during the deformation, a Neumann boundary condition [17] is applied in the contact region. The elastic force acting on the elastic particle is the same in magnitude as the elastic force acting on the rigid wall (i.e. Newton’s third law). Therefore, it is not necessary to integrate the stress field over the entire particle body to obtain the force; instead, the elastic force acting on the rigid wall is recorded.

The particle is discretized by using a fully unstructured mesh. A local grid refinement is adopted near the contact region as shown in Fig. 2. The particle can collide with the wall at three principal orientations: horizontal, vertical and oblique. The required grid resolution differs in each case. As illustrated in the mesh refinement study (see Fig. 3), the grid resolution of the oblique orientation is the finest, and more than 100,000 grid elements are needed for the simulation to obtain mesh independent results. For horizontal and vertical orientations, 50,000 grid elements are sufficient for the FE calculation as the contact regions are symmetric in both cases.

Particles of different material types are used in this study, as listed in Table 1. The spherical particle is used to verify the FE simulation results with the analytical solution of Eq. (3). To determine the unknown coefficients  $\xi$  and  $i$  in Eq. (6), type I of the prolate spheroid is used, and thus the current model is established. Type II and III of the prolate spheroids have different particle aspect ratios and material properties and are used to verify the established model.

### Numerical verification of finite element simulations

FE simulation results are first verified by comparison with the analytical solutions in the case of spherical particles for different particle sizes and materials as shown in Fig. 4. The difference in values  $\phi$  between the FE simulation results  $F_{e,FE}$  and the analytical results  $F_{e,an}$  is sufficiently small at small impact velocities, i.e.  $\phi = |F_{e,FE} - F_{e,an}| / F_{e,an} \leq 0.93\%$  for  $U_N \leq 0.2$ . Because the analytical model of Eq. (3) was derived based on the assumption of small particle

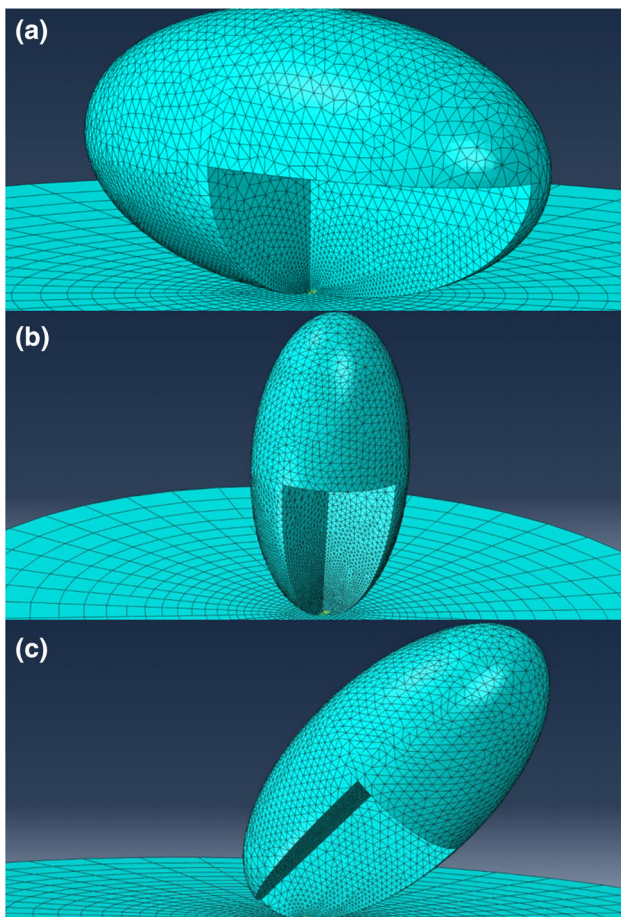


**Fig. 2** Local grid refinement of the prolate spheroidal particle at three principal orientations: horizontal (a), vertical (b) and oblique (c) ( $\lambda = 2$ )

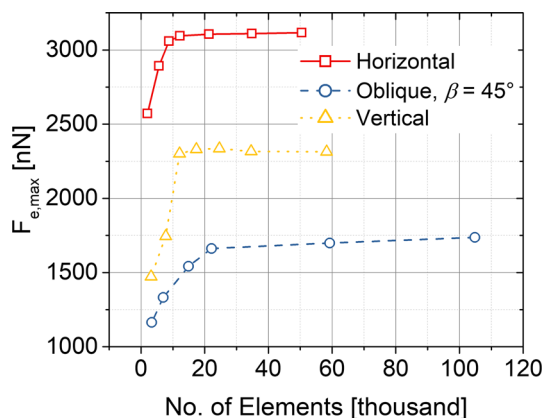


**Fig. 3** Mesh refinement study of the maximum elastic force acting on a prolate spheroidal particle during its collision with a plane wall by using unstructured meshes for three principal orientations ( $U_N = 0.1$  m/s,  $\rho_p = 2500$  kg/m<sup>3</sup>,  $E_p = 64$  GPa and  $\sigma_p = 0.24$ )

deformations. The difference in values increased significantly with increasing impact velocities;  $\phi$  reaches to 5.1% at  $U_N = 20$  m/s.

The magnitudes between the maximum elastic force, the fluid dynamic drag force and the gravity are compared in Fig. 5 (note that the ordinate axis is on a logarithmic scale). The drag force model used in this comparison is according to Schiller and Naumann [19]. The relative velocities used in both models are kept the same (i.e.  $|\mathbf{u}_p - \mathbf{u}_f| = U_N$ , where  $\mathbf{u}_p$  and  $\mathbf{u}_f$  are the particle velocity and the fluid velocity, respectively). Compared with the maximum elastic force, the drag force is 5000 times smaller, and the gravity is 158,000 times smaller. Therefore, it is reasonable to neglect the drag force and the gravitational force during the analysis of particle–wall collisions.

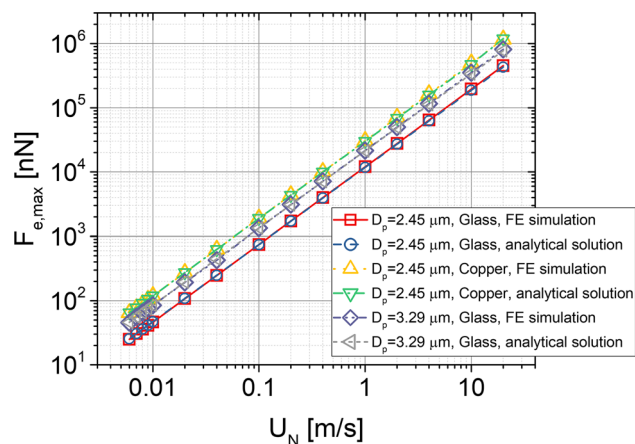
#### 4 Results analysis and determination of the elastic force model

Figure 6 plots the maximum elastic force acting on the prolate spheroidal particle for different particle aspect ratios and orientation angles. For all aspect ratios, the maximum elastic force is the greatest at the horizontal orientation angle (i.e.  $\beta = 0^\circ$ ) and then decreases with increasing orientation angle. At the orientation angle of  $45^\circ$ , the maximum elastic reaches the lowest value. After that, the maximum elastic force increases with increasing orientation angle and reaches another peak value at the vertical orientation angle (i.e.  $\beta = 90^\circ$ ). However, the maximum elastic force at the vertical orientation is still much lower than in the horizontal orientation case. Interestingly, it is found that all three curves (i.e. maximum elastic force as a function of the orientation angle for three different aspect ratios) have an intersection point at  $\beta = 5^\circ$  (see Fig. 6). Figure 7 plots the von Mises stress distribution at orientation angles of  $3^\circ$  and  $45^\circ$  for three different aspect ratios. The region that has the largest level of the von Mises stress distribution in the case of  $\beta = 3^\circ$  is larger than in the case of  $\beta = 45^\circ$ . The reason is that more kinetic energy of the particle can be transformed into elastic potential energy if the contact region becomes symmetric. In the case of  $\beta = 45^\circ$ , the deformation cannot fully develop as the particle can rotate around the contact region.

In order to calculate the coefficient  $i$  in Eq. (6), the particle size and material properties are kept constant. Only the normal impact velocity and the orientation angle are varied in the FE simulations. In this way, the terms of  $\rho^i$ ,  $D_p^2$  and  $\left[ E_p / \left[ 1 - \sigma_p^2 \right] \right]^{1-i}$  of Eq. (6) become constant values, and the maximum elastic force  $F_{e,max} \propto U_N^{2i}$ . Then the coefficient  $i$  can be calculated by fitting the curve of  $F_{e,max} = c U_N^{2i}$ , where  $c$  is a coefficient that relates to the particle shape, size and material properties. Figure 8 plots the maximum elastic force as a function of the normal impact velocity for different orientation angles. By fitting the curve of the simulation data for all orientation angles, it is found

**Table 1** Material properties of different types of particles

Particle types	Young's modulus [GPa]	Poisson's ratio [-]	Density [kg/m <sup>3</sup> ]	Volume equivalent diameter [μm]	Aspect ratio [-]
Sphere (E-glass)	80	0.22	2560	2.45, 3.29	1
Prolate spheroid type I (glass)	63	0.24	2500	2.45, 5, 10	1.5, 2, 3
Prolate spheroid type II (copper)	115	0.35	8960	2.45	2
Prolate spheroid type III (iron)	203	0.29	7690	2.45	1.5



**Fig. 4** Numerical verification of the FE simulated results by comparison with an analytical solution in the case of sphere-wall collision for different particle sizes and materials ( $\rho_p = 2560 \text{ kg/m}^3$ ,  $E_p = 80 \text{ GPa}$  and  $\sigma_p = 0.22$ )

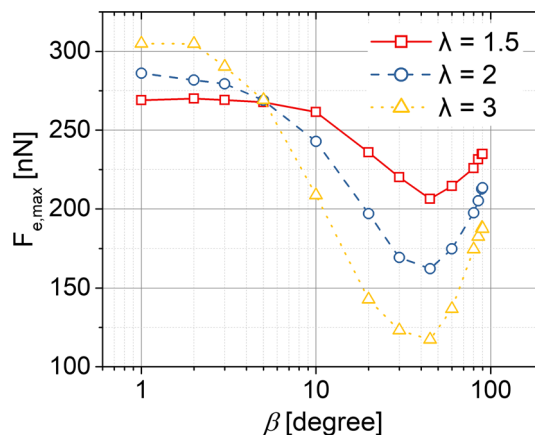


**Fig. 6** The influence of the orientation angle on the maximum elastic force acting on the prolate spheroidal particle for different particle aspect ratios ( $U_N = 0.0457 \text{ m/s}$ ,  $\rho_p = 2500 \text{ kg/m}^3$ ,  $E_p = 64 \text{ GPa}$  and  $\sigma_p = 0.24$ )

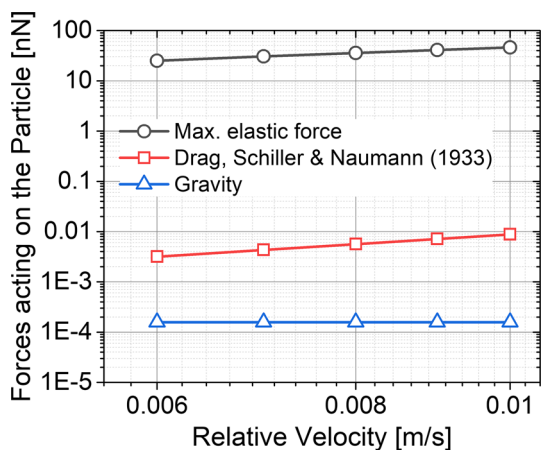


**Fig. 5** Comparison of the maximum elastic force, the drag force and the gravity acting on a spherical particle ( $D_p = 2.45 \text{ μm}$ ,  $\rho = 2560 \text{ kg/m}^3$ ,  $E_p = 80 \text{ GPa}$ ,  $\sigma_p = 0.22$ )

that the coefficient  $i$  remains a constant value of 0.6, which coincide with the analytical solution of the spherical particle. Therefore, Eq. (6) simplifies to

$$F_{e,\max} = \xi(\lambda, \beta) \rho_p^{0.6} U_N^{1.2} D_p^2 \left[ \frac{E_p}{1 - \sigma_p^2} \right]^{0.4} \quad (7)$$

The general expression of  $\xi(\lambda, \beta)$  is difficult to derive since both  $\lambda$  and  $\beta$  are dimensionless values. However, we should keep in mind that  $\xi(\lambda, \beta)$  is a constant value for any given particle aspect ratio and orientation angle. If the particle aspect ratio is fixed, the coefficient  $\xi$  is a function of the orientation angle, i.e.  $\xi(\lambda = \text{const}, \beta)$ . Therefore, it is possible to determine the function  $\xi(\lambda = \text{const}, \beta)$  for different particle aspect ratios. In this work, three particle aspect ratios are considered, i.e.  $\lambda = 1.5, 2, 3$ . Figure 9 plots the coefficient  $\xi$  as a function of the orientation angle for these three particle aspect ratios. By applying polynomial fitted curves on these data, the function  $\xi(\lambda = 1.5, 2 \text{ or } 3, \beta)$  can finally be obtained as

**Fig. 7** The instantaneous von Mises stress distribution of prolate spheroidal particles during the collision with a plane rigid wall for different particle aspect ratios ( $U_N = 0.0457$  m/s,  $\rho_p = 2500$  kg/m<sup>3</sup>,  $E_p = 64$  GPa and  $\sigma_p = 0.24$ )

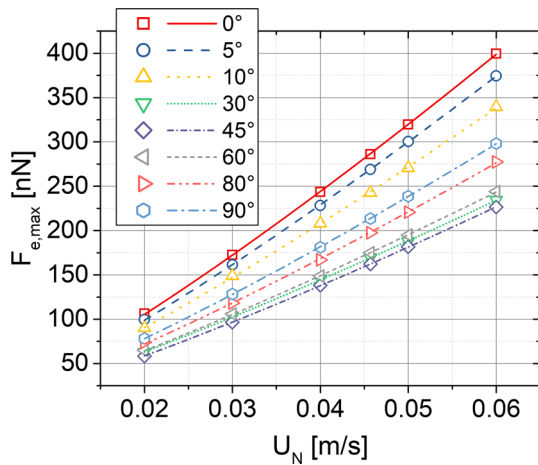
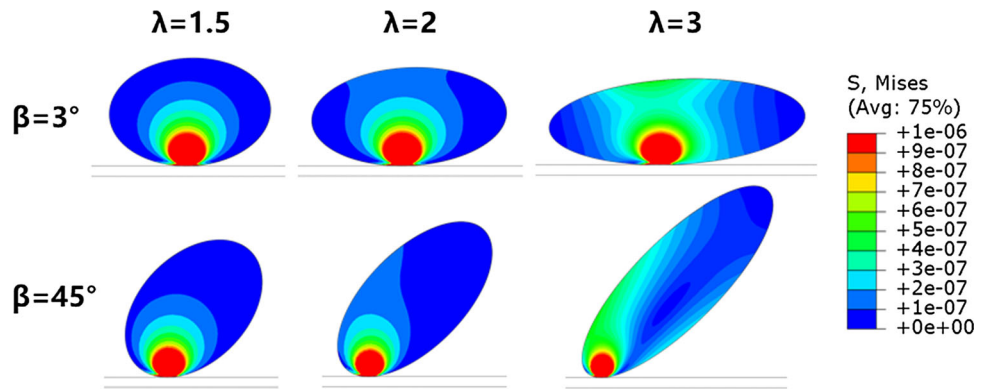


**Fig. 8** The influence of normal impact velocity on the maximum elastic force of the prolate spheroidal particle for different orientation angles ( $\rho_p = 2500$  kg/m<sup>3</sup>,  $E_p = 64$  GPa,  $\sigma_p = 0.24$ , and  $\lambda = 2$ )

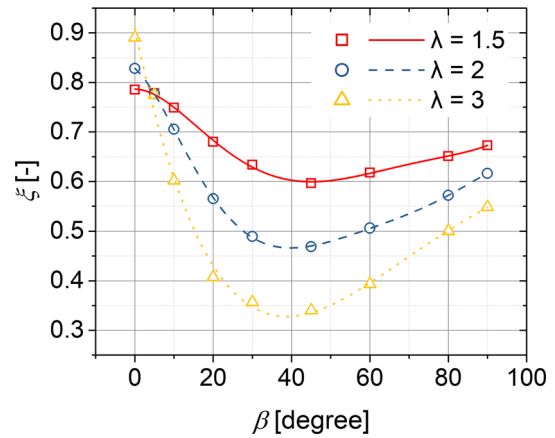


**Fig. 9** The influence of the orientation angle on the coefficient of  $\xi$  ( $\lambda = \text{const.}$ ,  $\beta$ ) for different aspect ratios ( $U_N = 0.0457$  m/s,  $\rho = 2500$  kg/m<sup>3</sup>,  $E_p = 64$  GPa and  $\sigma_p = 0.24$ )

$$\begin{bmatrix} \xi(\lambda = 1.5, \beta) \\ \xi(\lambda = 2, \beta) \\ \xi(\lambda = 3, \beta) \end{bmatrix} = \begin{bmatrix} 0.7864 & 0.82837 & 0.9087 \\ 8.2293 \times 10^{-5} & -0.00652 & -0.0377 \\ -5.2329 \times 10^{-4} & -9.7135 \times 10^{-4} & 8.1284 \times 10^{-4} \\ 1.6670 \times 10^{-5} & 4.6124 \times 10^{-5} & -6.6192 \times 10^{-6} \\ -1.9929 \times 10^{-7} & -8.1944 \times 10^{-7} & 1.9372 \times 10^{-8} \\ 9.5851 \times 10^{-10} & 6.6760 \times 10^{-9} & 0 \\ -1.1658 \times 10^{-12} & -2.0774 \times 10^{-11} & 0 \end{bmatrix}^T \begin{bmatrix} 1 \\ \beta \\ \beta^2 \\ \beta^3 \\ \beta^4 \\ \beta^5 \\ \beta^6 \end{bmatrix}. \quad (8)$$

Equations (7) and (8) are the proposed maximum elastic force model for prolate spheroidal particles. This model is straightforward and the functions of  $\xi(\lambda = 1.5, 2 \text{ or } 3, \beta)$  are explicitly given in this study. For other values of the aspect ratio  $\lambda$ , the user can follow the same FE simulation steps and construct a new function  $\xi(\lambda = \text{const.}, \beta)$ .

### Verification of the proposed elastic force model

First, the proposed model is compared with independent FE simulation results for different particle materials. Here, two types of particle materials are considered, i.e. copper and iron

(particle type II and III as listed in Table 1) [12]. In order to increase the difference between the two cases, the particle aspect ratio is also varied. The aspect ratios for particle type II and III are 2 and 1.5, respectively. Figure 10 compares the results between the proposed model and the FE simulation for different particle material types. The difference between the results is very small, proving the validity of the proposed model.

The proposed model is further verified by varying the particle size and aspect ratio. Two types of particles are compared:  $D_p = 5 \mu\text{m}$ ,  $\lambda = 2$ ; and  $D_p = 10 \mu\text{m}$ ,  $\lambda = 1.5$ .

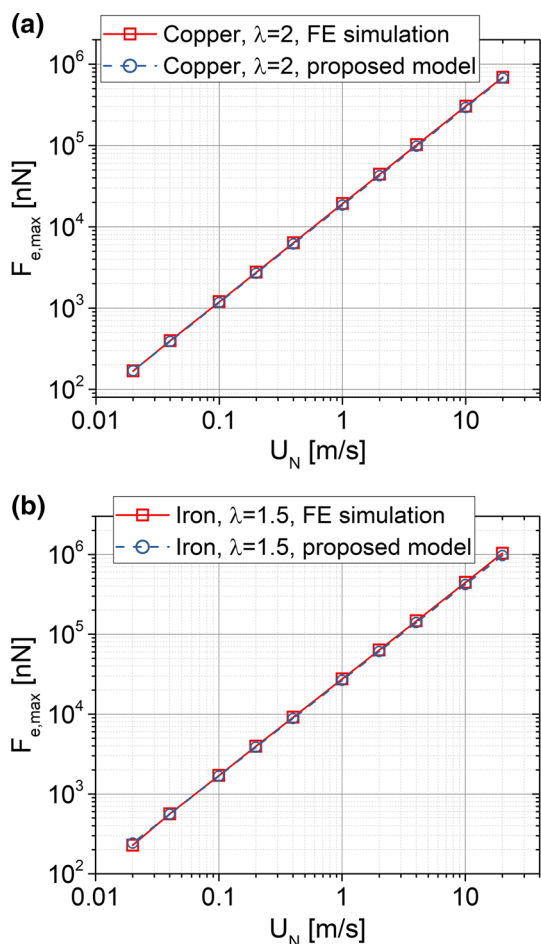


**Fig. 10** Comparison of the results calculated by using the proposed maximum elastic force model and independent FE simulations for different particle material properties and aspect ratios; **a** particle material: copper,  $\lambda = 2$ ; **b** particle material: iron,  $\lambda = 1.5$  ( $\beta = 45^\circ$ , particle material properties are listed in Table 1)

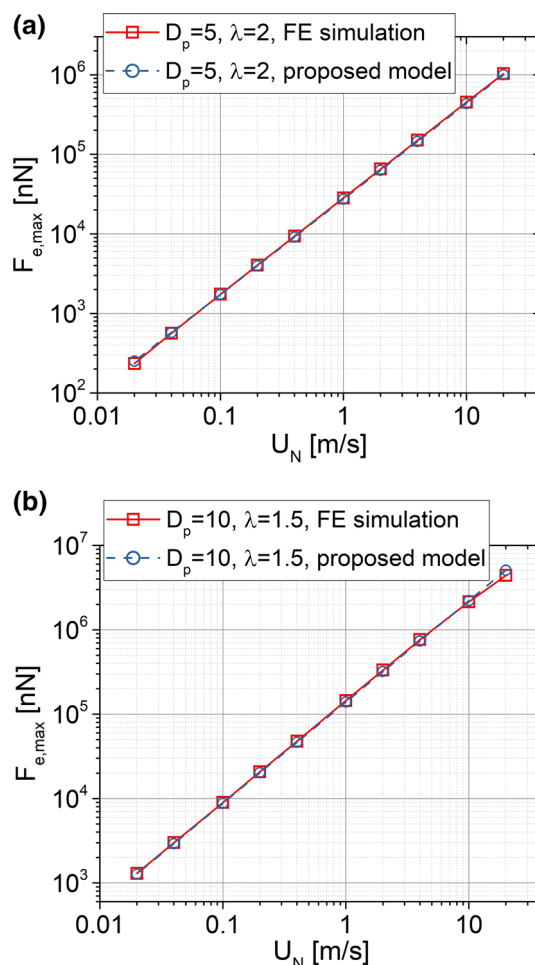


**Fig. 11** Comparison of the results calculated by using the proposed maximum elastic force model and independent FE simulations for different particle sizes and aspect ratios; **a**  $D_p = 5 \mu\text{m}$ ,  $\lambda = 2$ ; **b**  $D_p = 10 \mu\text{m}$ ,  $\lambda = 1.5$  ( $\beta = 45^\circ$ ,  $\rho_p = 2500 \text{ kg/m}^3$ ,  $E_p = 64 \text{ GPa}$  and  $\sigma_p = 0.24$ )

Figure 11 compares the results calculated by the present model and the FE simulation. In both cases, a good agreement between results is again found. However, as shown in Fig. 11b, the inertia of the particle becomes four times larger when the particle size is increased from 5 to 10  $\mu\text{m}$ , and therefore the difference in results reaches 13.6% at  $U_N = 20 \text{ m/s}$ . Finally, the proposed model is verified by varying both the particle orientation angle and the particle aspect ratio. As shown in Fig. 12, at  $\beta = 80^\circ$  and  $\lambda = 3$ , the difference in results between the proposed model and the independent FE simulation is very small.

The difference between the analytical solution and the FE simulation results increases with large particle deformation, as illustrated in Fig. 4. However, the threshold value of particle deformation varies from case to case and is influenced by the particle size and aspect ratio. Since the deformation decreases with increasing particle aspect ratio, it is reasonable to use the threshold value of particle deformation in the

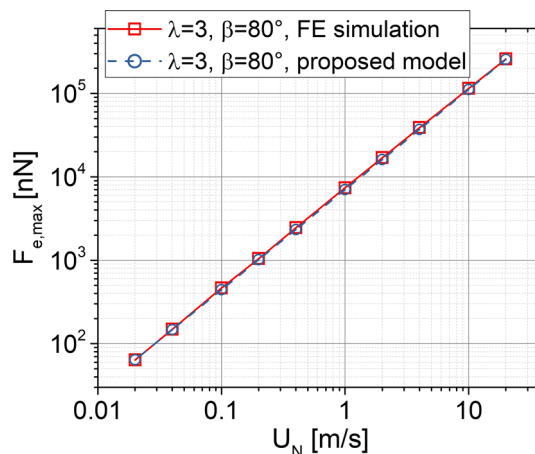


**Fig. 12** Comparison of the results calculated by using the proposed maximum elastic force model and independent FE simulations at aspect ratio  $\lambda = 3$  and orientation angle  $\beta = 80^\circ$  ( $D_p = 2.45 \mu\text{m}$ ,  $\rho_p = 2500 \text{ kg/m}^3$ ,  $E_p = 64 \text{ GPa}$  and  $\sigma_p = 0.24$ )

case of a spherical particle as a reference value. In all cases, if the analytical solution of Landau et al. [16] is applicable, the proposed force model can be applied as well.

## 5 Conclusions

In this work, a straightforward hybrid analytical–numerical model is proposed to calculate the maximum elastic force acting on an elastic prolate spheroidal particle during the collision with a solid plane wall. The generalised form of the model is derived through analogy arguments, and the number of coefficients of the model is reduced by using dimensional analysis. The remaining two unknown coefficients, i.e.  $i$  and  $\xi(\lambda, \beta)$ , are determined by performing FE simulations. It is found that the coefficient  $i = 0.6$  is constant for different particle orientation angles, which coincides with the analytical solution for spherical particles.  $\xi(\lambda, \beta)$  is solely a function of the particle aspect ratio and orientation angle. The functions of  $\xi(\lambda = \text{const}, \beta)$  at three different aspect ratios (i.e.  $\lambda = 1.5, 2$  and  $3$ ) are given in this study. Intense verifications have been performed by varying particle material properties, sizes and shapes. Good agreement between the results of the proposed model and the FE simulation was found in all cases. The proposed model can be used to calculate the maximum elastic force acting on a prolate spheroidal particle during the collision with a wall at small deformations of the particle for arbitrary properties of particle material, sizes, aspect ratios and orientation angles. This model can be easily implemented into a Lagrangian particle tracking algorithm and allows an accurate prediction of the elastic force of prolate spheroidal particles during their collision with a wall.

**Acknowledgements** The authors acknowledge the financial support by the Chinese Fundamental Research Funds for the Central Universities of the Project 2020kfyXJJS065; The authors also thank the Deutsche Forschungsgemeinschaft for the financial support in the framework of the Project STE 544/58 and the joint Chinese–Slovenian bilateral research Project BI-CN/20-22-002 funded by the Slovenian Research Agency and the Ministry of Science and Technology of China.

**Data availability** the data that support the findings of this study are available from the corresponding author upon reasonable request.

## Declarations

**Conflict of interest** The authors declare that there is no conflict of interest.

## References

- Almohammed N, Breuer M (2016) Modeling and simulation of particle–wall adhesion of aerosol particles in particle–laden turbulent flows. *Int J Multiph Flow* 85:142–156. <https://doi.org/10.1016/j.ijmultiphaseflow.2016.06.013>
- Ariane M, Sommerfeld M, Alexiadis A (2018) Wall collision and drug-carrier detachment in dry powder inhalers: using DEM to devise a sub-scale model for CFD calculations. *Powder Technol* 334:65–75. <https://doi.org/10.1016/j.powtec.2018.04.051>
- Cheung CS, Cao YH, Yan ZD (2005) Numerical model for particle deposition and loading in electret filter with rectangular split-type fibers. *Comput Mech* 35:449–458. <https://doi.org/10.1007/s00466-004-0634-5>
- Cui Y, Hu R, Ravnik J, Yinshui L, Zhou X, Hribersek M, Steinmann P (2021) Analysis of elastic force of fibres during the collision with a wall at arbitrary orientation angles: the importance of fibre’s secondary collision. Submitted to *Particuology*
- Cui Y, Ravnik J, Steinmann P, Hribersek M (2019) Settling characteristics of nonspherical porous sludge flocs with nonhomogeneous mass distribution. *Water Res* 158:159–170. <https://doi.org/10.1016/j.watres.2019.04.017>
- Cui Y, Sommerfeld M (2019) The modelling of carrier-wall collision with drug particle detachment for dry powder inhaler applications. *Powder Technol* 344:741–755. <https://doi.org/10.1016/j.powtec.2018.12.067>
- Fan F-G, Ahmadi G (1995) A sublayer model for wall deposition of ellipsoidal particles in turbulent streams. *J Aerosol Sci* 26:813–840. [https://doi.org/10.1016/0021-8502\(95\)00021-4](https://doi.org/10.1016/0021-8502(95)00021-4)
- Fang Z, Wang H, Zhang Y, Wei M, Wu X, Sun L (2019) A finite element method (FEM) study on adhesive particle–wall normal collision. *J Aerosol Sci* 134:80–94. <https://doi.org/10.1016/j.jaerosci.2019.04.018>
- Fang Z, Zhang Y, Wei M, Zhao S, Sun L, Wu X (2020) The critical sticking velocity of non-spherical graphite particles: a numerical study and validation. *Nucl Eng Des* 359:110453. <https://doi.org/10.1016/j.nucengdes.2019.110453>
- Fang Z, Zhang Y, Wei M, Zhao S, Wu X, Sun L (2020) A numerical study on adhesive collision between a micro-sized particle and a wall. *Powder Technol* 360:769–779. <https://doi.org/10.1016/j.powtec.2019.08.114>
- Feng Y, Kleinstreuer C (2013) Analysis of non-spherical particle transport in complex internal shear flows. *Phys Fluids* 25:091904. <https://doi.org/10.1063/1.4821812>
- Hentschel ML, Page NW (2006) Elastic properties of powders during compaction. Part 1: pseudo-isotropic moduli. *J Mater Sci* 42:1261–1268. <https://doi.org/10.1007/s10853-006-1145-x>
- Hu Y, Yao Z, Hu J (2009) An analytical model to predict residual stress field induced by laser shock peening. *J Manuf Sci Eng* 131:031017. <https://doi.org/10.1115/1.3139219>
- Johnson KL (1982) One hundred years of Hertz contact. *Proc Inst Mech Eng* 196:363–378. [https://doi.org/10.1243/pime\\_proc\\_1982\\_196\\_039\\_02](https://doi.org/10.1243/pime_proc_1982_196_039_02)
- Kosinski P, Hoffmann AC (2009) Extension of the hard-sphere particle–wall collision model to account for particle deposition. *Phys Rev E* 79:061302. <https://doi.org/10.1103/physreve.79.061302>
- Landau LD, Pitaevskii LP, Kosevich AM, Lifshitz EM (2012) *Theory of elasticity*. Elsevier Science, Amsterdam
- Logan JD (2013) *Applied mathematics*, 4th edn. Wiley, New York
- Parker G (1978) Self-formed straight rivers with equilibrium banks and mobile bed. Part 1. The sand-silt river. *J Fluid Mech* 89:109–125. <https://doi.org/10.1017/s0022112078002499>
- Schiller L, Naumann A (1933) Über die grundlegenden berchnungen beider schwerkraftaufbereitung. *Z. Ver. Deut. Ing.* 77:318–320
- Surhone LM, Tennoe MT, Henson SF (eds) (2010) *Dirichlet boundary condition*. Betascript Publishing, Riga
- Tian L, Ahmadi G, Wang Z, Hopke PK (2012) Transport and deposition of ellipsoidal fibers in low Reynolds number flows. *J Aerosol Sci* 45:1–18. <https://doi.org/10.1016/j.jaerosci.2011.09.001>
- Zhang K, Chanpura RA, Mondal S, Wu C-H, Sharma MM, Ayoub JA, Parlar M (2014) Particle size distribution measurement tech-

- niques and their relevance or irrelevance to sand control design. In: Day 1 Wed, February 26, 2014. SPE. <https://doi.org/10.2118/168152-ms>
23. Zhang Y, Fang Z, Zhao S, Wei M, Wu X, Sun L (2020) An experimental study on the wall collision of micro-sized graphite particles by high-speed photomicrography. *Prog Nucl Energy* 125:103391. <https://doi.org/10.1016/j.pnucene.2020.103391>
24. Zhao J, Dong Y, Ye C (2021) Optimization of residual stresses generated by ultrasonic nanocrystalline surface modification through analytical modeling and data-driven prediction. *Int J Mech Sci* 197:106307. <https://doi.org/10.1016/j.ijmecsci.2021.106307>

**Publisher's Note** Springer Nature remains neutral with regard to jurisdictional claims in published maps and institutional affiliations.